Structural basis and energy landscape for the Ca^{2+} gating and calmodulation of the Kv7.2 K^+ channel

Ganeko Bernardo-Seisdedos[a,b], Eider Nuñez[b], Carolina Gomis-Perez[b], Covadonga Malo[b], Álvaro Villarroel[b,1], and Oscar Millet[a,1]

[a]Protein Stability and Inherited Disease Laboratory, Center for Cooperative Research in Biosciences CIC bioGUNE, 48170 Derio, Spain; and [b]Instituto Biofisika (Consejo Superior de Investigaciones Científicas, Universidad del País Vasco), University of Basque Country, 48940 Leioa, Spain

Edited by Richard W. Aldrich, The University of Texas at Austin, Austin, TX, and approved January 24, 2018 (received for review January 10, 2018)

The Kv7.2 (KCNQ2) channel is the principal molecular component of the slow voltage-gated, noninactivating K^+ M-current, a key controller of neuronal excitability. To investigate the calmodulin (CaM)-mediated Ca^{2+} gating of the channel, we used NMR spectroscopy to structurally and dynamically describe the association of helices *h*A and *h*B of Kv7.2 with CaM, as a function of Ca^{2+} concentration. The structures of the CaM/Kv7.2-hAB complex at two different calcification states are reported here. In the presence of a basal cytosolic Ca^{2+} concentration (10–100 nM), only the N-lobe of CaM is Ca^{2+}-loaded and the complex (representative of the open channel) exhibits collective dynamics on the millisecond time scale toward a low-populated excited state (1.5%) that corresponds to the inactive state of the channel. In response to a chemical or electrical signal, intracellular Ca^{2+} levels rise up to 1–10 μM, triggering Ca^{2+} association with the C-lobe. The associated conformational rearrangement is the key biological signal that shifts populations to the closed/inactive channel. This reorientation affects the C-lobe of CaM and both helices in Kv7.2, allosterically transducing the information from the Ca^{2+}-binding site to the transmembrane region of the channel.

ion channel | calmodulin | calcium regulation | Kv7 potassium channel | M-current

Voltage-gated K^+ channels are responsible for the ion fluxes that regulate the electrical signaling in excitable cells such as neurons, cardiac myocytes, auditory cells, or vascular smooth muscle cells (1, 2). In turn, such channels are often controlled by the temporal and spatial modulation of the intracellular (i) Ca^{2+} concentration, which can vary from 100 nM in resting cells up to 1–10 μM (local $[Ca^{2+}]_i$) (3). Calcium regulation of a K^+ channel may occur through direct Ca^{2+} association with a cytosolic domain of the channel (3, 4), or, more frequently, it can be mediated by calmodulin (CaM), the primary Ca^{2+} sensor in eukaryotic cells (5, 6).

CaM regulation of ion channels (calmodulation) is a process well understood thermodynamically, which often involves tuning Ca^{2+} affinities from the CaM lobes upon complexation (7). From the structural point of view, an allosteric mechanism is required to propagate Ca^{2+} signaling from the cytosol up to the transmembrane region (8). The rich complexity of functional states accessible for ionic channels suggests that measurable conformational transitions are likely responsible for calmodulation signal propagation. However, despite the large repository of high-resolution structures of CaM bound to ion channel fragments (6), the mechanism for this allosteric event has not yet been reported for any channel.

Here, we have investigated the Ca^{2+}-dependent conformational landscape of the voltage-gated and Ca^{2+}-regulated K^+ channel Kv7.2. In combination with Kv7.3, it conforms the molecular components of the M-current (9), which is opened at subthreshold membrane potentials, providing a brake for membrane excitation (10, 11). To close the channel and regulate the M-current, Kv7.2 is sensitive to the Ca^{2+} release after bradykinin activation in sympathetic neurons (12, 13). Kv7.2 is sensitive to Ca^{2+} only after it binds to CaM at the specific binding motif located in helix A (IQ motif) (Fig. S1*A*), which can occur in the presence or absence of the metal ion (14, 15). Thus, Kv7.2 regulation by Ca^{2+} is a representative example of ion channel modulation by CaM.

The Kv7 family has been investigated using X-ray crystallography: The structure of the chimeric Kv7.2/7.3 cytosolic region (*h*A and *h*B in Fig. S1*A*) complexed with CaM (16) and the structures of equivalent moieties for the homologous channels Kv7.1 (17) and CaM complexed with helix *h*B of Kv7.4 (18) are available. Despite the obvious interest of such structural instances, a thorough study of the conformational landscape of Ca^{2+} gating is missing. Using NMR spectroscopy, we have characterized the structure and dynamics of *h*AB of Kv7.2 in complex with CaM (263 residues in total) at different Ca^{2+} saturation states. In the absence of added Ca^{2+}, the protein complex structure is loaded with two Ca^{2+} ions in the N-lobe of CaM. In this intermediate Ca^{2+} state, the complex undergoes extensive dynamics on the millisecond time scale, affecting backbone and side chains. Intriguingly, Ca^{2+} saturation and/or depletion results in the disappearance of the dynamics and is accompanied by a structural rearrangement, particularly noticeable in the Ca^{2+}-loaded state. Collective analysis of the structural instances, the modulated Ca^{2+} affinities of CaM upon binding Kv7.2-*h*AB, and the protein dynamics provides an unprecedented view of the energy landscape of calmodulation and a structural model for the allosteric rearrangement associated with the Ca^{2+} gating of a Kv7 channel.

Significance

Ion channels are sophisticated proteins that exert control over a plethora of body functions. Specifically, the members of the Kv7 family are prominent components of the nervous systems, responsible for the ion fluxes that regulate the electrical signaling in neurons and cardiac myocytes. Albeit its relevance, there are still several questions, including the Ca^{2+}/calmodulin (CaM)-mediated gating mechanism. We found that Ca^{2+} binding to CaM triggers a segmental rotation that allosterically transmits the signal from the cytosol up to the transmembrane region. NMR-derived analysis of the dynamics demonstrates that it occurs through a conformational selection mechanism. Energetically, CaM association with the channel tunes the affinities of the CaM lobes (calmodulation) so that the channel can sense the specific changes in $[Ca^{2+}]$ resulting after an action potential.

Author contributions: Á.V. and O.M. designed research; G.B.-S., E.N., and C.G. performed research; C.M. contributed new reagents/analytic tools; G.B.-S. analyzed data; and Á.V. and O.M. wrote the paper.

The authors declare no conflict of interest.

This article is a PNAS Direct Submission.

Data deposition: The NMR chemical shifts have been deposited in the BioMagResBank, www.bmrb.wisc.edu (accession nos. 34097 and 34226) and in the Protein Data Bank, www.wwpdb.org (PDB ID codes 6FEG and 6FEH).

[1]To whom correspondence may be addressed. Email: alvaro.villarroel@csic.es or omillet@cicbiogune.es.

This article contains supporting information online at www.pnas.org/lookup/suppl/doi:10.1073/pnas.1800235115/-/DCSupplemental.

Published online February 20, 2018.

Results

Finding Soluble and Functional Constructs of Kv7.2-*h*AB. The expression of the cytosolic moiety of Kv7.2 covering helices *h*A and *h*B (Fig. S1*B*) results in an insoluble and aggregated protein. We identified a hydrophobic region prone to be unstructured and to suffer from proteolysis and generated a construct of the Kv7.2 C terminus that encloses helices *h*A and *h*B (residues Q310–R532) with the linker deletion ΔR374–K493 (Kv7.2-*h*AB[Δ6L]; Fig. S1*B*). Bacterial coexpression of Kv7.2-*h*AB[Δ6L] with CaM results in a monodisperse protein complex. Experimental evidence supports the biological relevance of this construct: The interlink region between helices *h*A and *h*B is not required for channel function or assembly (19), and electrophysiological recordings of cells expressing Kv7.2-*h*AB[WT] and Kv7.2-*h*AB[Δ6L] demonstrate that the average current density and Boltzmann parameters are comparable in both channels (Fig. S1 *C* and *D*). Altogether, it can be concluded that the Kv7.2-*h*AB[Δ6L] construct (henceforth Kv7.2-*h*AB) represents a bona fide and meaningful model that retains all of the functional properties of the channel fragment.

Solution Structure of the CaM/Kv7.2-*h*AB Complex in the Absence of Added Ca^{2+}. The solution structure of the CaM/Kv7.2-*h*AB complex in the absence of added Ca^{2+} was determined by NMR spectroscopy. First, chemical shift assignments were achieved using orthogonal isotopic labeling (Fig. S2) to alleviate signal overlap, and more than 95% of the ^{1}H, ^{15}N, and ^{13}C (backbone) resonances were assigned [BioMagResBank (BMRB) accession no. 34097; Fig. S2].

The Ca^{2+} association state with the CaM/Kv7.2-*h*AB complex was investigated using the ^{1}H, ^{15}N chemical shift perturbations (CSPs) as reporters of the ion effect. Upon Ca^{2+} saturation, the vast majority of the CaM-perturbed residues belong to the EF hands located in the C-lobe of CaM, with no significant CSPs in the N-lobe (Fig. 1*A*, yellow bars). Ca^{2+} depletion of the complex with EGTA produces exactly the mirror effect (Fig. 1*A*, red bars). Thus, in the absence of added Ca^{2+}, Kv7.2-*h*AB associates with CaM at an intermediate Ca^{2+} state in which only its N-lobe is loaded. This is consistent with the crystallographic structure of the CaM/Kv7.1-*h*AB complex (17), where CaM is also Ca^{2+}-loaded just in the N-lobe. We will refer to this partially Ca^{2+}-loaded complex as "intermediate" *int*CaM/Kv7.2-*h*AB.

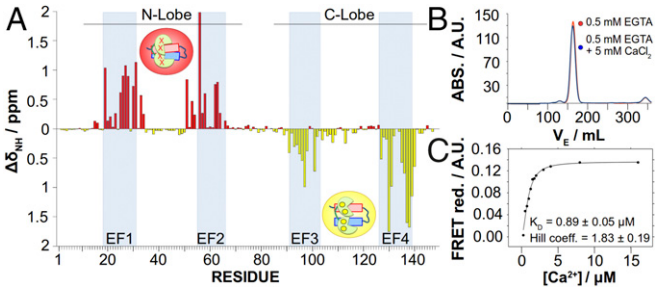

Fig. 1. CSPs induced by Ca^{2+} over CaM complexed with helices A and B. (*A*) CSP analysis of residues forming CaM. The *apo*CaM/Kv7.2-*h*AB complex shows large CSPs in the EF1 and EF2 hands, whereas *holo*CaM/Kv7.2-*h*AB shows large CSPs in the EF3 and EF4 hands, demonstrating that *int*CaM/Kv7.2-*h*AB is Ca^{2+}-loaded in the N-lobe, whereas the C-lobe is Ca^{2+}-free. $\Delta\delta_{NH}$, absolute amide chemical shift differences. (*B*) Size exclusion chromatography profiles after injecting samples with and without Ca^{2+} in a Superdex 26/60 column. Elution peaks for the *apo*- and *holo*CaM/Kv7.2-*h*AB complexes (30.27 kDa) are almost identical (162.66 mL and 163.896 mL, respectively), corresponding to a theoretical molecular mass of 31.13 kDa and 30.3 kDa, respectively. ABS., absorbance; V_E, eluted volume. (*C*) Ca^{2+} titration curve for the CaM/Kv7.2-*h*AB complex. Ca^{2+} affinity is measured by FRET ratio reduction between the mTFP1 (donor) and mVenus (acceptor) fluorophores located in the N and C termini of the Kv7.2-*h*AB construct complexed with CaM. The EC_{50} value (equivalent to an apparent K_d for the C-lobe) is 0.89 ± 0.05 μM, and the Hill coefficient is h = 1.83 ± 0.19 as obtained from the fitting to a Hill equation: $EC_{50} = F_\infty \cdot [Ca^{2+}]^h / (EC_{50}^h + [Ca^{2+}]^h)$, where EC_{50} corresponds to the concentration of Ca^{2+} at which FRET change is half-maximal, h is the Hill coefficient, and $F_\infty$is the FRET change found at a large excess of free calcium.

The 3D structure of the *int*CaM/Kv7.2-*h*AB complex in solution [Protein Data Bank (PDB) ID code 6FEG; Fig. 2 *A* and *B* and Fig. S4] was calculated employing 5,981 NOEs, 306 dihedral angles, and 134 residual dipolar couplings (RDC) restraints (Table S1). The protein complex shows helices *h*A and *h*B wrapped by CaM (Fig. 2 *A* and *B*). A third helix composed of residues H357–R365 (*h*TW in Fig. 2*B*) is located in the flexible linker between helices *h*A and *h*B, and it does not make significant contacts with the rest of the protein complex. The *pre-h*A region (16, 17) is partially unstructured in *int*CaM/Kv7.2-*h*AB (Fig. 2*B*), but this is likely due to the channel truncation. The complex is structurally similar to the available PDB entries of CaM complexed to other Kv7 subunits (Fig. S3), showing rmsd values of 1.07 Å with the CaM/Kv7.1-*h*AB complex (17) and 1.4 Å with the CaM/Kv7.2-*h*A/Kv7.3-*h*B chimera (16), while it shows fewer similarities with the Ca^{2+}-loaded CaM/Kv7.4-*h*AB complex (18) (rmsd = 8.1 Å, mostly due to a segmental rearrangement).

The Structural Basis of CaM/Kv7.2-*h*AB Ca^{2+} Gating. Ca^{2+} saturation of the CaM/Kv7.2-*h*AB complex results in CSPs in the Kv7.2-*h*AB moiety as well. To investigate the putative conformational changes as a function of Ca^{2+}, we have investigated the structural properties of CaM/Kv7.2-*h*AB at two other concentrations of this ion. The "apo" form (devoid of Ca^{2+}, *apo*CaM/Kv7.2-*h*AB) and the fully loaded Ca^{2+} complex (*holo*CaM/Kv7.2-*h*AB) were purified and found to be stable over time. The hydrodynamic radius and the stoichiometry of the complexes do not vary with [Ca^{2+}], as shown by the elution profile from size exclusion chromatography (Fig. 1*B*), indicating that the ion-dependent structural variations are subtle, in agreement with the moderate CSPs of CaM/Kv7.2-*h*AB with [Ca^{2+}] (Fig. S2). A structural model from *apo*CaM/Kv7.2-*h*AB was obtained based on these chemical shift changes combined with ^{1}J(N-H) residual dipolar couplings in an aligned medium. The resulting *apo*CaM/Kv7.2-*h*AB model (Fig. 2*C*) is similar to the partially Ca^{2+}-loaded *int*CaM/Kv7.2-*h*AB complex, showing variations in the flexible regions (including the EF-hand loops as discussed below) and, to a lesser extent, in the *h*AB interhelical orientation.

The solution structure of the *holo*CaM/Kv7.2-*h*AB complex was also determined by NMR spectroscopy (Fig. 2 *D* and *E* and Fig. S4). The assigned chemical shifts (94% of the ^{1}H, ^{15}N, and ^{13}C; BMRB accession no. 34226), a set of NOEs (n = 5,287), and RDCs (n = 131) were used to resolve the 3D fold of the protein complex (PDB ID code 6FEH). Even though the main structural features are maintained, the helices *h*A and *h*B have changed their relative disposition and *holo*CaM/Kv7.2-*h*AB is conformationally different from the existing structures, with rmsd values of 3.3 Å, 3.7 Å, and 9.3 Å for the CaM/Kv7.1-*h*AB complex (17), CaM/Kv7.2-*h*A/Kv7.3-*h*B chimera (16) and CaM/Kv7.4-*h*AB complex (18), respectively (Fig. S3). More importantly, *holo*CaM/Kv7.2-*h*AB also significantly differs from *int*CaM/Kv7.2-*h*AB (rmsd = 3.1 Å), but the two structures can be reconciled by a segmental rearrangement (Fig. 2*F*): Ca^{2+} association with CaM produces a 17.9° rotation of the EF hands, which also pulls helices *h*8 and *h*5 of CaM and helix *h*A of Kv7.2. Remarkably, as a result of the segmental solid-rigid rotation, the *h*AB helices have changed the interhelical angle and their relative orientation with respect to CaM. Altogether, such torsion is the necessary (and sufficient) rearrangement to explain the allosteric transmission from the Ca^{2+}-binding site of the CaM's C-lobe up to the helix *h*A (and to the *pre-h*A) of Kv7.2.

All of the experiments were run at 120 mM KCl, and under these close-to-physiological conditions, the N-lobe of CaM in the complex binds Ca^{2+} with extremely high affinity. Actually, *apo*CaM/Kv7.2-*h*AB can only exist in the presence of a

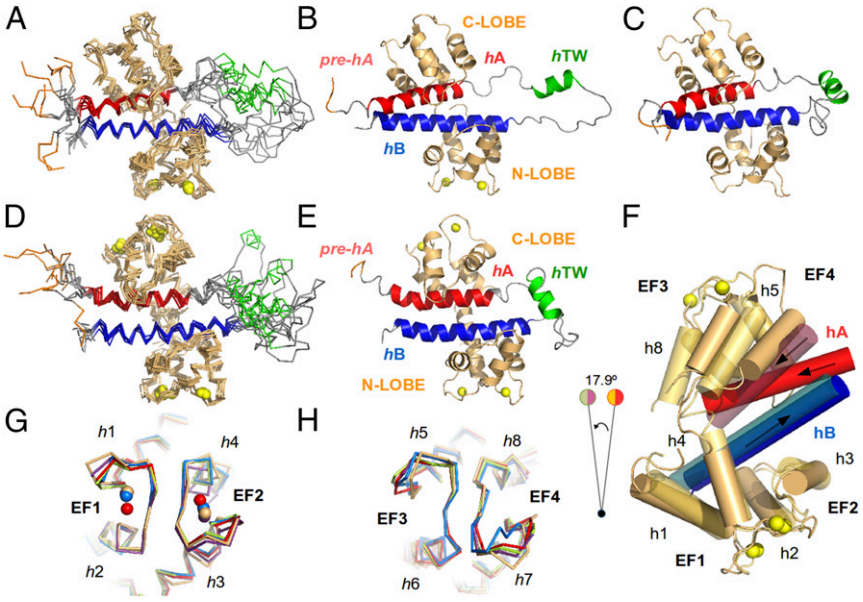

Fig. 2. Structure of the CaM/Kv7.2-*h*AB complex at different calcification states. An overlay of the 10 lowest energy conformers representing the 3D solution structure of the *int*CaM/Kv7.2-*h*AB (*A*) or *holo*CaM/Kv7.2-*h*AB (*D*) complex is shown. A ribbon representation of the *int*CaM/Kv7.2-*h*AB (*B*) or *holo*CaM/Kv7.2-*h*AB (*E*) complex shows the structural elements: CaM protein (orange); the prehelix A(*pre-h*A), which connects segment 6 of the pore with the rest of the intracellular C terminus of the Kv7.2 channel (purple); helix *h*A (red); helix *h*TW (green); and helix *h*B (blue). Ca^{2+} ions are represented as spheres. The same color code is used for the ribbon representations of the *apo*CaM/Kv7.2-*h*AB complex. (*C*) Ribbon representation of the structural model of the *apo*CaM/Kv7.2-*h*AB complex. (*F*) Alignment of *int*CaM/Kv7.2-*h*AB and *holo*CaM/Kv7.2-*h*AB by the center of mass of the N-lobe of CaM displays the rotation (17.9°) of a segment of the complex upon Ca^{2+} binding to the C-lobe of CaM. The involved structural elements are *h*5 and *h*8 in CaM and *h*A in Kv7.2-*h*AB. (*G*) Alignment of the EF-hand motifs of the N-lobe of *int*CaM/Kv7.2-*h*AB (orange) with the equivalent motif in other reported (Ca^{2+}-loaded) CaM structures: 4RJD (purple), 4UMO (blue), 4GOW (red), and 5J03 (green), with rmsd values of 1.12 Å, 1.22 Å, 1.26 Å, and 1.39 Å, respectively. (*H*) Alignment of the EF-hand motifs of the C-lobe of *int*CaM/Kv7.2-*h*AB (orange) with the equivalent motif in other reported (apo) CaM structures: 4V0C (blue), 4E50 (red), 4JQ0 (purple), and 5J03 (green), with rmsd values of 0.93 Å, 0.94 Å, 1.18 Å, and 1.25 Å, respectively.

large excess of a strong Ca^{2+} chelating agent (i.e., EGTA), and the Ca^{2+} affinity for the N-lobe is estimated to be subnanomolar ($K_d < 10^{-3}$ μM). This is in contrast to free CaM, where the C-lobe shows the highest affinity for the ion (K_d[C-lobe] = 3.4 μM, K_d[N-lobe] = 14 μM) (20). On the other hand, the Ca^{2+} affinity for the C-lobe in *int*CaM/Kv7.2-*h*AB has been determined by fluorescence resonance energy transfer (FRET): When two independent fluorophores are attached to Kv7.2-*h*AB, the above-mentioned Ca^{2+}-gated conformational rearrangement produces a change in the FRET intensity (Fig. 1*C*). The FRET intensity as a function of the free Ca^{2+} concentration (as determined by fura-2) (21) provides an apparent affinity constant of 0.89 ± 0.05 μM, consistent with other determinations in similar constructs (22). The Hill coefficient of 1.83 suggests that the event is monitoring the saturation of CaM's C-lobe with two ion units.

Both CaM lobes in CaM/Kv7.2-*h*AB show altered affinity with respect to free CaM (calmodulation), and we focused on the conformation adopted by the EF-hand loops, since they are responsible for Ca^{2+} association. Compared with the available crystallographic (Fig. 2*G*) and solution (Fig. S5) structures of CaM, the N-terminal EF-hand loops of *apo*CaM/Kv7.2-*h*AB agree better with Ca^{2+}-bound conformations. Moreover, the interhelical angle analysis (6) (Table S2) also suggests that the lobe is already in a "holo" (Ca^{2+}-bound) conformation, providing a structural explanation for the increase in affinity. However, this mechanistic explanation is constrained by the validity of the structural model of *apo*CaM/Kv7.2-*h*AB, based on a limited number of experimental restraints (chemical shifts and RDCs). On the other hand, the EF hands of the C-lobe of *int*CaM/Kv7.2-*h*AB have interhelical angles characteristic of a partially open conformation (Table S2), and the conformation is similar to *apo*CaM structures (Fig. 2*H* and Fig. S5). These results are consistent with the moderate affinity increase and the micromolar K_d range observed for the C-lobe in the complex.

The Conformational Changes Are also Observed upon Tetramerization. To validate whether the observed changes are also present in a tetrameric architecture, we looked for Ca^{2+}-dependent conformational changes in a channel moiety that includes the regions responsible for tetramerization (helices *h*C and *h*D of the cytosolic C-lobe of Kv7.2; Fig. S1*A*). The $^{1}H,^{15}N$–transverse relaxation optimized spectroscopY (TROSY)–heteronuclear single quantum spectroscopy (HSQC) of the CaM/Kv7.2-*h*ABCD (Fig. S2) shows only a few peaks corresponding to residues from flexible regions, in good agreement with the spectrum of a tetrameric structure of more than 120 kDa. Instead, the methyl-TROSY spectrum (23) of the ^{13}C–δ-Ile methyl groups of *int*CaM/Kv7.2-*h*ABCD displays the vast majority of residues. Despite the signal overlap, the superposition of *int*CaM/Kv7.2-*h*ABCD and *int*CaM/Kv7.2-*h*AB spectra (Fig. 3*A*) allows the assignment of the *h*AB δ-Ile residues in *int*CaM/Kv7.2-*h*ABCD. Noticeably, the spectrum for *holo*CaM/Kv7.2-*h*ABCD shows the same Ca^{2+}-induced CSP as *holo*CaM/Kv7.2-*h*AB (Fig. 3*A*), indicating that the ion-dependent conformational changes are maintained in the tetrameric complex.

FRET experiments provide further evidence that the Ca^{2+}-dependent conformational changes are also present in the tetrameric complex. Fig. 3 *B* and *C* shows how FRET analysis is sensitive to the conformational change occurring in the transition between *apo*CaM/Kv7.2-*h*AB (solid red line) and *holo*CaM/Kv7.2-*h*AB (dashed red line). The magnitude of such change is maintained in the *int*CaM/Kv7.2-*h*ABCD complex (Fig. 3*C* and green lines in Fig. 3*B*), while no change in the FRET signal can be detected when using a CaM mutant unable to bind Ca^{2+} (CaM[1234]; blue lines in Fig. 3 *B* and *C*).

***int*CaM/Kv7.2-*h*AB Shows Excursions to an Excited State, Compatible with *holo*CaM/Kv7.2-*h*AB.** Analysis of the conformational ensemble obtained after the experimental restraint refinement indicates

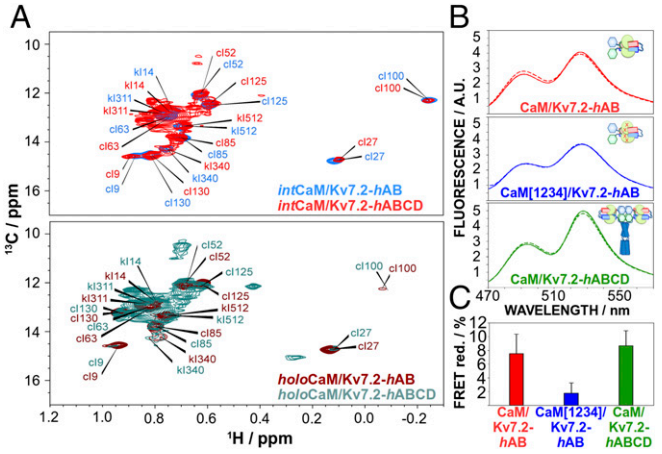

Fig. 3. Conformational changes are also observed in tetrameric channel constructs. (*A*) ^{13}C–δ-Ile region of the methyl-TROSY spectrum for *int*CaM/Kv7.2-*h*AB (blue, *Top*), *int*CaM/Kv7.2-*h*ABCD (red, *Top*), *holo*CaM/Kv7.2-*h*AB (brown, *Bottom*), and *holo*CaM/Kv7.2-*h*ABCD (green, *Bottom*). The monomeric complex (CaM/Kv7.2-*h*AB) and the tetrameric assembly (CaM/Kv7.2-*h*ABCD) experience the same conformational changes triggered by Ca^{2+}. The assignment of the methyl peaks in *int*CaM/Kv7.2-*h*AB was achieved by a combination of multiple 3D experiments, while the same peaks in *int*CaM/Kv7.2-*h*ABCD are estimated by spectra overlap. (*B*) mTFP1 (Donor) and mVenus (Acceptor) are localized in the N and C termini of helices AB, respectively. CaM/Kv7.2-*h*AB (*Top*, red), CaM[1234]/Kv7.2-*h*AB (*Middle*, blue), and CaM/Kv7.2-*h*ABCD (*Bottom*, green) emission spectra in the absence (full line) and presence (dashed line) of Ca^{2+}-saturating concentrations are shown. (*C*) FRET reduction ratios relative to the maximum excitation (~492 nm) and emission (~526 nm) peaks. Ca^{2+} addition induces noticeable conformational changes (similar in magnitude) in the monomeric version (CaM/Kv7.2-*h*AB) or the tetrameric version (CaM/Kv7.2-*h*ABCD), but not for the CaM[1234]/Kv7.2-*h*ABCD tetramer.

that the *int*CaM/Kv7.2-*h*AB protein complex may undergo intermolecular flexibility. NMR is especially suitable for the characterization of protein motions at multiple time scales, and for motions in the microsecond-to-millisecond time scale, the relaxation-dispersion (RD) experiment allows a full description of the exchange process, providing an estimation for the exchange rate (k_{ex}) and the population (p_B)/chemical shift (Δδ) of the excited state (24). Backbone amide RD experiments collected at two magnetic fields identified pervasive dynamics in CaM's C-lobe region of *int*CaM/Kv7.2-*h*AB, with measurable line broadening ranging between 1.5 and 20 Hz (Fig. 4). The individual fitting of the RD profiles shows a high degree of consistency in the obtained parameters (homogeneous k_{ex} and p_B values), so a collective fitting was attempted. Dynamic residues could be initially clustered into three different groups (groups I–III; Fig. S6) with robust statistics (Table S3). Group I entails five residues included in the construct but not corresponding to coding regions of the channel, so it is not considered further. Group II encloses 15 residues belonging to helices *h*A, *h*B, and *h*TW of Kv7.2. Most of the residues in group II face the C-lobe of CaM, whose dynamic residues are clustered in group III. Remarkably, group II and III residues can be interpreted using equivalent fitting parameters (Table S3), suggesting that the *int*CaM/Kv7.2-*h*AB may undergo intermolecular concerted dynamics. Groups II and III are well described by a single motional event of 1.1 ± 0.2 ms, with an excited state of 1.5 ± 0.6% (Table S3).

The region of the complex that experiences conformational dynamics (Fig. 4) agrees well with the segmental motion upon Ca^{2+} association with the C-lobe of CaM/Kv7.2-*h*AB (Fig. 2*F*). Moreover, the RD-fitted Δδ values show an excellent correlation with the CSP upon Ca^{2+} addition to *int*CaM/Kv7.2-*h*AB (Fig. S6*D*). Equivalent experiments were repeated for the *apo*- and *holo*CaM/Kv7.2-*h*AB states. In both cases, the dynamic residues conforming the conformational exchange (dynamic residues from groups II and III) are abrogated. Thus, we conclude that *int*CaM/Kv7.2-*h*AB undergoes excursions toward an excited state compatible with *holo*CaM/Kv7.2-*h*AB. This conformational exchange is not originated from the in and out transfer of residual Ca^{2+} ions to the CaM-binding site since equivalent line broadening is obtained when the RD experiments are repeated in the presence of an excess of EGTA (Fig. S6*G*). Instead, the collective motion seems to be originated by an incomplete electrostatic cancellation from the acidic CaM and the basic Kv7.2-*h*AB subunits. In this hypothesis, line broadening is drastically attenuated when the ionic strength is increased (up to 500 mM KCl; Fig. S6*F*). This electrostatic complementarity has also been previously observed for CaM binding to its binding domain in the SK channel (25), among other systems (26).

We also investigated the dynamic properties of the δ-Ile methyl groups, which are widespread throughout the protein complex (Fig. 3*A*). There are three methyl groups (out of 12) showing dynamics in the *int*CaM/Kv7.2-*h*AB complex, but not in the *apo*- or *holo*CaM/Kv7.2-*h*AB complex (Fig. 4), indicating that side chains are equally sensing the collective dynamics of the complex. Thus, our results demonstrate that changes in Ca^{2+} concentration result in modulation of the dynamic behavior of the protein complex, with two resting states (*apo*CaM/Kv7.2-*h*AB and *holo*CaM/Kv7.2-*h*AB) and a highly dynamic and interconverting state (*int*CaM/Kv7.2-*h*AB).

Discussion

Ca^{2+} gating of K^+ channels mediated by CaM is responsible for the tight control of a plethora of subcellular functions (27). However, the Ca^{2+} regulation mechanism for such voltage-dependent channels has remained, to the best of our knowledge, ill-defined since the first CaM-binding epitopes were identified. So far, the most accurate structural description of a Ca^{2+}-gated regulation mechanism comes from the SK2 channels (25, 28, 29), where it has been demonstrated that Ca^{2+} binding to CaM produces a large conformational change that includes bridging different channel subunits. In Kv7 channels, it has been long hypothesized that Ca^{2+} regulation is also driven by conformational changes derived from the interaction between Ca^{2+} and CaM, and Minor and coworkers (18) suggested that CaM's conformational change could be the mechanical switch required to open/close the pore depending on the Ca^{2+} levels. In this paper, we provide extensive experimental evidence that such conformational change does indeed occur, providing an estimation of the energy landscape and a structural model for the allosteric rearrangement associated with the Ca^{2+} gating of the Kv7.2 channel.

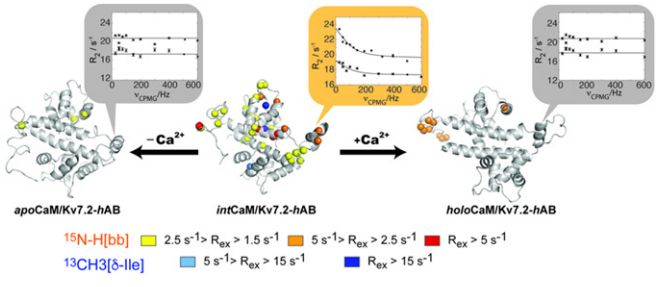

Fig. 4. Millisecond dynamics of intCaM/Kv7.2-*h*AB populate the holoCaM/Kv7.2-*h*AB state to a low extent. In the structure, the spheres pinpoint the ^{15}N-H backbone (bb) amide groups and ^{13}C–δ-Ile methyl groups that are experiencing microsecond-to-millisecond dynamics for the three conformations under consideration. The magnitude of the exchange line broadening is color-coded as indicated. The vignettes show a representative example of the RD profiles (Val366). The solid lines correspond to the fitting to the Carver–Richards equation, simultaneously, of the two static magnetic field datasets (600 and 800 MHz).

We report the conformational instances of the CaM/Kv7.2 complex with atomic resolution at the two calcification states plus a structural model of a third state, covering all of the intracellular physiological concentrations, from 10–100 nM at the resting state up to 1–10 μM after chemical or electrical signaling: *apo*CaM/Kv7.2-*h*AB (Ca^{2+} unloaded), *int*CaM/Kv7.2-*h*AB (loaded in the N-lobe of CaM), and *holo*CaM/Kv7.2-*h*AB (full Ca^{2+}-loaded). In the three cases, the structures show a very intimate complex in a 1:1 stoichiometry where CaM wraps the Kv7.2 helices that are forming an antiparallel coiled-coil: Helix *h*A is bound to the *apo*–C-lobe of CaM, whereas helix *h*B is making contact with the Ca^{2+}-loaded N-lobe. This result is largely consistent with the crystallographic structures of the CaM/Kv7.1-*h*AB and CaM/Kv7.3-*h*A/Kv7.2-*h*B complexes reported by Hirsch and coworkers (16, 17).

The reported conformational instances conceal the dynamic transitions required to define the conformational/energy landscape associated with Ca^{2+} gating of the channel (energy landscape of Fig. 5 and Movie S1). The *apo*CaM/Kv7.2-*h*AB complex exists only in the presence of strong chelating agents. Moreover, *apo*CaM/Kv7.2-*h*AB results in an open complex according to *in cellulo* M-current recordings with a CaM variant unable to chelate the ion (CaM^{1234}; Fig. 5). Since the basal Ca^{2+} concentration of the neuronal cytosol is around 100 nM, we conclude that this conformation should be only theoretical and not found intracellularly. On the other hand, *int*CaM/Kv7.2-*h*AB is structurally rather similar and, energetically at least, 7 kcal·mol^{-1} more stable than *apo*CaM/Kv7.2-*h*AB (as estimated from the change in K_d values), also maintaining the channel in the open state. The existence of different conformations that result in an open channel underscores that the conformational plasticity in the N-lobe may be required for putative interactions with other secondary messengers (i.e., phosphatidylinositol biphosphate) (30) to further modulate the gating of the channel.

From the functional point of view, the key step is the transition from *int*CaM/Kv7.2-*h*AB to *holo*CaM/Kv7.2-*h*AB: Ion binding to the C-lobe concertedly displaces a segment of CaM (helices *h*5 and *h*8), which is allosterically transmitted to the channel moiety by modifying the orientation of helices *h*A and *h*B (Fig. 2*F*). We hypothesize that this conformational change is mechanically transmitted to the intramembranous region of the channel through a change in orientation of the *pre-h*A element, gating the closing of the channel and, ultimately, resulting in M-current depletion. Such change is energetically favored at about 1 kcal·mol^{-1}, which ensures the reversibility of the system upon disappearance of the signaling Ca^{2+} concentration.

The above-mentioned states are not isolated conformations only connected by the (increasing) Ca^{2+} concentration; rather, they are also intrinsically coupled through thermal motions. The RD experiments show pervasive dynamics in CaM's C-lobe of *int*CaM/Kv7.2-*h*AB, which can be adequately described as a collective motion of the complex. In the most simple and widespread interpretation of the RD experiment, the two-state model chemical shift analysis demonstrates that *int*CaM/Kv7.2-*h*AB is sensing a low-populated state (1.5% at 303 K), which corresponds to the *holo*CaM/Kv7.2-*h*AB state. Such dynamics are likely originated by an insufficient electrostatic complementarity between the (acidic) CaM and the (basic) Kv7.2-*h*AB in *int*CaM/Kv7.2-*h*AB, which becomes fully satisfied (and the millisecond dynamics largely quenched) when an excess of Ca^{2+} locks the complex in the *holo*CaM/Kv7.2-*h*AB state. From the functional point of view, the preexisting equilibrium of populations is a consequence of the (low) energy barrier between the states, and Ca^{2+} association with *int*CaM/Kv7.2-*h*AB implies a conformational selection mechanism instead of a more canonically induced fit. Conformational selection is widely used by nature, and has been reported in many enzymes (31) and binding proteins (32), including CaM (33), and it is most efficient to produce an allosteric response after a stimulus (34).

The results presented here are also able to explain the role of CaM and the calmodulation mechanism associated with the Ca^{2+} gating of the Kv7.2 channel (Fig. 5). At any ion concentration, the Kv7.2-*h*AB complex subunit cannot be purified in the absence of CaM due to aggregation followed by precipitation. Moreover, CaM's affinity for the channel is so high that the complex cannot be dissociated by any of the in vitro-tested conditions. Likely, this is also the case in vivo, due to the high intracellular concentration of CaM (10^{-6}–10^{-5} M) (5). Together, these results suggest that CaM association with Kv7.2 may become consubstantial to the channel's integrity once both molecules interact. This situation is similar to the homologous channel Kv7.1, where a constitutive binding role was hypothesized (17), and to other proteins like phosphorylate kinase (5). In any case, CaM association with Kv7.2 results in a significant alteration of the Ca^{2+} affinities of the two lobes, sensitizing the CaM-effector complex to the specific $[Ca^{2+}]$ in the different neuronal states. At the structural level, such changes in affinity are consistent with the conformational changes observed in the EF hands of CaM/Kv7.2-*h*AB, compared with free CaM (Fig. 2 *F* and *G* and Table S2). The N-lobe of free CaM has a low affinity for calcium (20), which is drastically increased upon association with Kv7.2 ($K_d < 10^{-3}$ μM in *apo*CaM/Kv7.2-*h*AB; Fig. 5). Considering that the basal Ca^{2+} concentration in the neuron is around 100 nM, the N-lobe should always be Ca^{2+}-loaded. On the other hand, the C-lobe of CaM also alters its affinity for Ca^{2+} upon binding to Kv7.2 (Fig. 5), lowering its apparent K_d from 3.4 μM (for free CaM and at this ionic strength) (20) down to 0.9 μM in the *int*CaM/Kv7.2-*h*AB complex. This affinity tuning is required for the complex to rest inactive until an agonist-induced increase in the intracellular Ca^{2+} concentration occurs (up to 1–10 μM; Fig. 5). The higher $[Ca^{2+}]$ shifts the equilibrium toward the *holo*CaM/Kv7.2-*h*AB conformation, with the subsequent

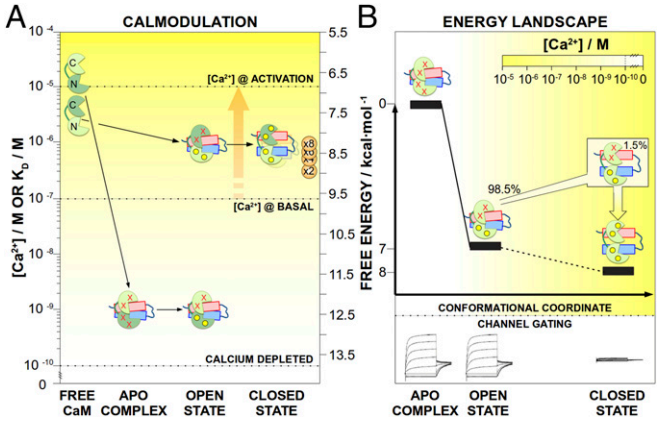

Fig. 5. Energy landscape and calmodulation of Kv7.2. The energy landscape and calmodulation connect the two different states of the channel: the open state (*apo*CaM/Kv7.2-*h*AB and *int*CaM/Kv7.2-*h*AB complexes) and the closed state (*holo*CaM/Kv7.2-*h*AB complex). In both panels, $[Ca^{2+}]$ is visualized by the yellow color intensity, as indicated in the inset scale. (*A*) Cartoons representing the different molecules are located in the ordinate axis according to the affinities of the dark green lobes. For instance, the N-lobes of CaM change their K_d for Ca^{2+} from 14 μM (free) to a K_d of less than 10^{-3} μM after complexation with Kv7.2-*h*AB (calmodulation). The horizontal dotted lines indicate the two different intracellular concentrations (the basal concentration and the maximum concentration induced by bradykinin), as well as a level that can be considered ion-free (Ca^{2+} depleted). The bradykinin-mediated Ca^{2+} release (orange arrow) triggers the transition from the open state toward the closed state of the channel. The apparent affinity of the channel for Ca^{2+} depends on the number of ions required to trigger the conformational change (from one to eight), as indicated by the orange circles. (*B*) Ca^{2+} affinities are used to estimate the relative energy levels of the different conformations, underlining the progressive stabilization of the complex with the Ca^{2+}-binding coordinate. In the *int*CaM/Kv7.2-*h*AB complex, the main population is in the open state, while a small population (1.5%) is already in the closed state.

conformational change that is allosterically transmitted up to the *pre-h*A element and likely to the transmembrane region, ultimately resulting in the closing of the channel.

Finally, it is worth considering the implications that channel tetramerization may have on the mechanisms introduced here. The methyl-TROSY spectra of the CaM/Kv7.2-*h*ABCD complex demonstrate that the same conformational states are maintained after channel tetramerization of the C terminus (Fig. 3*A*), while FRET experiments prove that Ca^{2+} triggers a conformational change in the tetrameric protein. According to our model, four CaM units will bind the cytosolic moiety of a full channel, generating a double number of putative loci for Ca^{2+} association (in the C-lobe). An unsolved question is how many Ca^{2+} units are needed to trigger the allosteric motion that will close the channel. Depending on the required number of ion units, the effective sensitivity of the channel for the ion concentration varies within the range of 0.9 μM (eight Ca ions per channel unit) up to 200 nM (two Ca ion per channel unit), as shown in Fig. 5.

In summary, in this contribution, we have presented a plethora of experimental data to support an unprecedented model for the Ca^{2+} gating of the potassium channel Kv7.2, which includes a complete description of the conformational landscape, the calmodulation mechanism, and a hypothesis on how Ca^{2+} can regulate the M-current in neurons. It is our belief that these results are of broader applicability to other Ca^{2+}-gated K^+ channels as well.

Methods

Expression and Purification of the CaM/Kv7.2-*h*AB Complex. The Kv7.2-*h*AB segment (residues 316–532) with the deletion ΔR374-K493 [Δ6L] was purified as previously described (20).

NMR Spectroscopy and Structure Calculation. NMR data were collected at 303 K on an 800-MHz Bruker Avance III spectrometer equipped with a cryoprobe and on a 600-MHz Bruker Avance III US2 spectrometer. Resonance assignments were obtained by the combined use of ^{15}N-HSQC, ^{13}C-HSQC, HNCA, HNcoCA, HNcaCB, HNcocaCB, HNCO, HNcaCO, HNHA, HNcaHA, HccoNH, and HNCccoNH experiments. NOE connectivities were obtained using ^{15}N–NOESY-HSQC and ^{13}C–NOESY-HSQC (120-ms mixing time, 16-ns rotation correlation time). Residual dipolar coupling was extracted by using TROSY ^{15}N-HSQC and semi-TROSY ^{15}N-HSQC experiments in isotropic and anisotropic (C12E5/1-hexanol) conditions. Protein complex structure was determined using ARIA2 (35). Transversal RD experiments were always acquired at two fields (600 MHz and 800 MHz) using a relaxation compensated-pulse Carr-Purcell-Meiboom-Gill sequence (CPMG) sequence (80 μs of total CPMG time) and variable effective fields: 25, 50(×2), 75, 100, 125, 150, 200, 250, 325, 400(×2), 500, 600, 700, 800, 900, and 1,000 Hz.

Electrophysiological Recordings. For the WT constructs, all experiments were carried out using HEK293T cells (HEK 293T/17, CRL-11268; American Type Culture Collection). The data were acquired at a sampling rate of 1 kHz and filtered at 100 Hz, and were analyzed using pCLAMP software (version 8.2; Axon Instruments) and plotted using SigmaPlot.

FRET Experiments. All FRET experiments were carried using an AMINCON Bowman series 2 luminescence fluorimeter. The fluorescence emission spectra of the proteins at 500 nM were collected over 470–570 nM after excitation at 458 nm (4-nm bandwidth). The FRET index was calculated as the ratio between the emission at 485–490 nm for the blue donor and the emission at 520–525 nm for the yellow acceptor. The total protein in each condition was assessed by direct excitation of the yellow protein at 520 nm, collecting the emission at 520–570 nm.

ACKNOWLEDGMENTS. Support was provided from the Department of Industry, Tourism and Trade of the Government of the Autonomous Community of the Basque Country (Grant Elkartek BG2015) and from the Ministry of Science and Technology Ministerio de Economía, Industria y Competitividad (Grants CTQ2015-68756-R, BFU2015-66910-R and CSD2008-00005).

1. Jespersen T, Grunnet M, Olesen S-P (2005) The KCNQ1 potassium channel: From gene to physiological function. *Physiology (Bethesda)* 20:408–416.
2. Sanguinetti MC, et al. (1996) Coassembly of K(V)LQT1 and minK (IsK) proteins to form cardiac I(Ks) potassium channel. *Nature* 384:80–83.
3. Berkefeld H, et al. (2006) BKCa-Cav channel complexes mediate rapid and localized Ca^{2+}-activated K^+ signaling. *Science* 314:615–620.
4. Miranda P, Giraldez T, Holmgren M (2016) Interactions of divalent cations with calcium binding sites of BK channels reveal independent motions within the gating ring. *Proc Natl Acad Sci USA* 113:14055–14060.
5. Chin D, Means A-R (2000) Calmodulin: A prototypical calcium sensor. *Trends Cell Biol* 10:322–328.
6. Villarroel A, et al. (2014) The ever changing moods of calmodulin: How structural plasticity entails transductional adaptability. *J Mol Biol* 426:2717–2735.
7. Tadross M-R, Dick I-E, Yue D-T (2008) Mechanism of local and global Ca^{2+} sensing by calmodulin in complex with a Ca^{2+} channel. *Cell* 133:1228–1240.
8. Haitin Y, Attali B (2008) The C-terminus of Kv7 channels: A multifunctional module. *J Physiol* 586:1803–1810.
9. Jentsch T-J (2000) Neuronal KCNQ potassium channels: Physiology and role in disease. *Nat Rev Neurosci* 1:21–30.
10. Hernandez C-C, Zaika O, Tolstykh G-P, Shapiro M-S (2008) Regulation of neural KCNQ channels: Signalling pathways, structural motifs and functional implications. *J Physiol* 586:1811–1821.
11. Soldovieri M-V, Miceli F, Taglialatela M (2011) Driving with no brakes: Molecular pathophysiology of Kv7 potassium channels. *Physiology (Bethesda)* 26:365–376.
12. Cruzblanca H, Koh D-S, Hille B (1998) Bradykinin inhibits M current via phospholipase C and Ca^{2+} release from IP_3-sensitive Ca^{2+} stores in rat sympathetic neurons. *Proc Natl Acad Sci USA* 95:7151–7156.
13. Gamper N, Shapiro M-S (2003) Calmodulin mediates Ca^{2+}-dependent modulation of M-type K^+ channels. *J Gen Physiol* 122:17–31.
14. Bal M, Zaika O, Martin P, Shapiro M-S (2008) Calmodulin binding to M-type K^+ channels assayed by TIRF/FRET in living cells. *J Physiol* 586:2307–2320.
15. Kosenko A, Hoshi N (2013) A change in configuration of the calmodulin-KCNQ channel complex underlies Ca^{2+}-dependent modulation of KCNQ channel activity. *PLoS One* 8:e82290.
16. Strulovich R, Tobelaim W-S, Attali B, Hirsch J-A (2016) Structural insights into the M-channel proximal C-terminus/calmodulin complex. *Biochemistry* 55:5353–5365.
17. Sachyani D, et al. (2014) Structural basis of a Kv7.1 potassium channel gating module: Studies of the intracellular c-terminal domain in complex with calmodulin. *Structure* 22:1582–1594.
18. Xu Q, Chang A, Tolia A, Minor D-L, Jr (2013) Structure of a $Ca^{(2+)}$/CaM:Kv7.4 (KCNQ4) B-helix complex provides insight into M current modulation. *J Mol Biol* 425:378–394.
19. Aivar P, et al. (2012) Surface expression and subunit specific control of steady protein levels by the Kv7.2 helix A-B linker. *PLoS One* 7:e47263.
20. Linse S, Helmersson A, Forsén S (1991) Calcium binding to calmodulin and its globular domains. *J Biol Chem* 266:8050–8054.
21. Grynkiewicz G, Poenie M, Tsien RY (1985) A new generation of Ca^{2+} indicators with greatly improved fluorescence properties. *J Biol Chem* 260:3440–3450.
22. Alaimo A, et al. (2014) Pivoting between calmodulin lobes triggered by calcium in the Kv7.2/calmodulin complex. *PLoS One* 9:e86711.
23. Wiesner S, Sprangers R (2015) Methyl groups as NMR probes for biomolecular interactions. *Curr Opin Struct Biol* 35:60–67.
24. Ortega G, Pons M, Millet O (2013) Protein functional dynamics in multiple timescales as studied by NMR spectroscopy. *Adv Protein Chem Struct Biol* 92:219–251.
25. Schumacher M-A, Rivard A-F, Bächinger H-P, Adelman J-P (2001) Structure of the gating domain of a Ca^{2+}-activated K^+ channel complexed with Ca^{2+}/calmodulin. *Nature* 410:1120–1124.
26. André I, Kesvatera T, Jönsson B, Linse S (2006) Salt enhances calmodulin-target interaction. *Biophys J* 90:2903–2910.
27. Adelman J-P, Maylie J, Sah P (2012) Small-conductance Ca^{2+}-activated K^+ channels: Form and function. *Annu Rev Physiol* 74:245–269.
28. Halling D-B, Kenrick S-A, Riggs A-F, Aldrich R-W (2014) Calcium-dependent stoichiometries of the KCa2.2 (SK) intracellular domain/calmodulin complex in solution. *J Gen Physiol* 143:231–252.
29. Zhang M, Pascal J-M, Zhang J-F (2013) Unstructured to structured transition of an intrinsically disordered protein peptide in coupling Ca^{2+}-sensing and SK channel activation. *Proc Natl Acad Sci USA* 110:4828–4833.
30. Tobelaim W-S, et al. (2017) Competition of calcified calmodulin N lobe and PIP2 to an LQT mutation site in Kv7.1 channel. *Proc Natl Acad Sci USA* 114:E869–E878.
31. Eisenmesser E-Z, et al. (2005) Intrinsic dynamics of an enzyme underlies catalysis. *Nature* 438:117–121.
32. Ortega G, Castaño D, Diercks T, Millet O (2012) Carbohydrate affinity for the glucose-galactose binding protein is regulated by allosteric domain motions. *J Am Chem Soc* 134:19869–19876.
33. Hoang J, Prosser R-S (2014) Conformational selection and functional dynamics of calmodulin: A (19)F nuclear magnetic resonance study. *Biochemistry* 53:5727–5736.
34. Vega S, Abian O, Velazquez-Campoy A (2016) On the link between conformational changes, ligand binding and heat capacity. *Biochim Biophys Acta* 1860:868–878.
35. Rieping W, et al. (2007) ARIA2: Automated NOE assignment and data integration in NMR structure calculation. *Bioinformatics* 23:381–382.